RSC Advances

PAPER

View Article Online
View Journal | View Issue

Cite this: *RSC Adv.*, 2021, **11**, 31015

A new PLA–Tween composited drug-carrying C60–Fe_3O_4 multifunctional ultrasound contrast agent based on three kinds of lesions

Baoqing Gao,†[a] Yao Feng,†[b] Xinmeng Chen[a] and Jie Zhang *[a]

A PLA–Tween composited drug-carrying C60–Fe_3O_4 microbubble was designed and prepared. Using Fe_3O_4 as a targeting factor and C60 as a drug carrier, warfarin (WF), netimixin (NET) and doxorubicin (DOX) respectively were loaded on a C60–Fe_3O_4 complex through π–π conjugate effect, and C60–Fe_3O_4–WF, C60–Fe_3O_4–NET and C60–Fe_3O_4–DOX targeted drug-loading complexes were obtained. The three drug-loading complexes were respectively combined into PLA and Tween membrane material, PLA–Tween composited C60–Fe_3O_4–DOX microbubbles, PLA–Tween composited C60–Fe_3O_4–NET microbubbles and PLA–Tween composited C60–Fe_3O_4–WF microbubbles were obtained, respectively. The average particle size of PLA–Tween composited drug-carrying C60–Fe_3O_4 microbubbles was 446.4 nm, the microbubble size was uniform, and the Zeta potential was −40.5 mV which showed a good stability. The loading rates of DOX, NET and WF in PLA–Tween composited drug-carrying C60–Fe_3O_4 microbubbles were 5.58%, 8.15% and 3.37%, respectively. PLA–Tween composited C60–Fe_3O_4–DOX microbubbles could inhibit the breast cancer MDA-MB-231 cells and normal mouse fibroblast 3T3 cells, the inhibition rates were respectively 53.4% and 18.6%, which significantly reduced the toxicity of free DOX drug on the normal cells (62.2%). PLA–Tween composited C60–Fe_3O_4–NET microbubbles had a inhibitory effect on the growth of *Staphylococcus aureus* and *Escherichia coli*, and the inhibitory effect on *Escherichia coli* was better. PLA–Tween composited C60–Fe_3O_4–WF microbubbles could inhibit the formation of thrombus, and PT, TT and APTT were significantly prolonged. PLA–Tween composited C60–Fe_3O_4 microbubbles had a developing effect on the kidney, bladder and abdominal aorta of rabbit. Under the action of external magnetic field, the ultrasonic imaging effect of composite microbubbles was significantly enhanced.

Received 25th June 2021
Accepted 29th August 2021

DOI: 10.1039/d1ra04936d

rsc.li/rsc-advances

An ultrasound contrast agent is a kind of preparation containing microbubbles of high concentration, it can not only diagnose by the use of ultrasonic imaging, but also promote thrombolysis and gene transfection, treat tumors and carry out a targeted drug delivery *in vivo*, *etc.* Due to the cavitation effect caused by the blasting of microbubbles under the ultrasound, targeted drug delivery carried by ultrasound contrast agent or non-invasive treatment is an important research direction in the biomedical field at present.[1,2]

Thrombosis results from a clot formed inside a blood vessel and it can block the blood flow, a serious thrombosis situation can lead to death and poses a serious threat to human health. Ultrasonic imaging can judge the conditions in the blood vessels and provide a basis for a further treatment, and it plays an increasingly important role in the examination and treatment of thrombosis diseases.[3–5] Common cystitis is an inflammatory lesion of the bladder caused by bacterial infection and is a potential precancerous lesion,[6,7] it is often found in middle-aged women and early diagnosis and treatment is particularly important. At present, the application of ultrasonic contrast agent in the study of bladder inflammation is relatively rare and has great research potential. Malignant tumor is one of the diseases that seriously threaten human health. Although the common tumor therapy drugs can inhibit the growth of tumor cells, they also have great toxic and side effects on the normal cells. Ultrasonic contrast agent microbubbles can burst under the ultrasound, which will produce a cavitation effect. Thus, if microbubbles carried the tumor therapy drugs were used for the targeted drug delivery on the lesion site, they would have a great potential in the treatment of tumor diseases. Loverlock *et al.*[8] studied the effect of continuous ultrasound on the doxorubicin cytotoxicity, and ultrasound can significantly enhance the inhibitory effect of doxorubicin on the tumor cells. Umemura *et al.*[9] studied the effect of ultrasonic radiation superposition on the mouse liver, the combination of ultrasonic radiation and

[a]*Heilongjiang Provincial Key Laboratory of New Drug Development and Pharmacotoxicological Evaluation, Jiamusi University, Jiamusi 154007, China. E-mail: zjie612@163.com; Tel: +86 13845455520*

[b]*First Affiliated Hospital, Jiamusi University, Jiamusi 154007, China*

† Baoqing Gao and Yao Feng contributed equally to this work.

drug administration could effectively improve the inhibition of drugs on tumors.

Fullerene (C60) has excellent physical and chemical properties such as small particle size, large specific surface area, low biotoxicity, good compatibility, good antibacterial and optical properties. When C60 was used as a drug carrier, its excellent properties made it more and more be applied in biology.[10,11] Fe_3O_4 nanoparticle has the characteristics of good stability, strong targeting, good biocompatibility and low toxicity, and simple preparation process. As a fine targeting factor, Fe_3O_4 nanoparticle had a wide range of applications in the field of biomedicine.

Excellent biological properties of C60 and the magnetic property of Fe_3O_4 were combined in this study, they were loaded with drug and then applied to ultrasound contrast agent. A multifunctional ultrasound contrast agent that integrated the targeted therapy and clinical observation was obtained.

1. Experiment

1.1 Preparation and characterization of C60–Fe_3O_4 magnetically targeted complex

C60 was dispersed in an appropriate of distilled water under the ultrasound. 0.47 g $FeCl_3$ and 0.23 g $FeCl_2$ were fully dissolved in a small amount of distilled water, then they were mixed with C60 suspension liquid. 1 mL PEG1500 solution (1 mg mL^{-1}) was added into above system and stirred at 60 °C. At the same time, NaOH solution with the concentration of 4 mg mL^{-1} was used to detect the acidity and alkalinity of the reaction solution. When the reaction solution was alkalinity, NaOH solution was stopped, the temperature of the system was raised to 80 °C and the reaction was continued for 0.5 h. After the reaction, C60–Fe_3O_4 magnetic targeted complex was obtained by repeated washing and freeze-drying.

1.2 Preparation of C60–Fe_3O_4 targeted drug delivery complex

1.2.1 C60–Fe_3O_4 loaded with doxorubicin. DOX standard curve: the content of DOX was determined by UV spectrophotometry. The standard solutions of DOX with concentrations of 2.5 μg mL^{-1}, 5 μg mL^{-1}, 10 μg mL^{-1}, 20 μg mL^{-1}, 30 μg mL^{-1}, 40 μg mL^{-1} and 50 μg mL^{-1} were obtained with anhydrous ethanol as solvent, respectively. The absorbance of each sample was determined by UV spectrophotometer at 480.0 nm with anhydrous ethanol as blank control. The linear regression equation of DOX was obtained by linear regression with absorbance value *A* as the ordinate and DOX concentration (μg mL^{-1}) as the abscissa.

C60–Fe_3O_4 loaded with doxorubicin: 15 mg C60–Fe_3O_4 complex and 22.5 mg DOX were placed in anhydrous ethanol, stirred at 35 °C for 4 h, filtered and dried, and C60–Fe_3O_4–DOX complex was obtained.

1.2.2 C60–Fe_3O_4 loaded with netilmicin. NET standard curve: the content of NET was obtained by using high performance liquid chromatography (HPLC). Mixture system of potassium dihydrogen phosphate (pH = 2.2) : acetonitrile = 75 : 25 was used as a mobile phase. NET standard solutions with concentrations of 10 μg mL^{-1}, 25 μg mL^{-1}, 50 μg mL^{-1}, 100 μg mL^{-1}, 200 μg mL^{-1}, 400 μg mL^{-1} and 600 μg mL^{-1} were obtained with the mobile phase as solvent. Under the flow rate of 1.0 mL min^{-1}, the column temperature of 30 °C and the injection volume of 10 μL, the peak area was detected at 205 nm. The linear regression equation of NET was obtained with the peak area as the ordinate and NET concentration (μg mL^{-1}) as the abscissa.

C60–Fe_3O_4 loaded with netilmicin: 15 mg C60–Fe_3O_4 complex and 30 mg NET were placed in a distilled water. The mixture was stirred at 40 °C for 2 h. After filtration and drying, C60–Fe_3O_4–NET complex was obtained.

1.2.3 C60–Fe_3O_4 loaded with warfarin. WF standard curve: the content of WF was obtained by HPLC. A mixture system of acetonitrile : water : acetic acid = 70 : 30 : 1 was the mobile phase. WF standard solutions with concentrations of 10 μg mL^{-1}, 25 μg mL^{-1}, 50 μg mL^{-1}, 100 μg mL^{-1}, 150 μg mL^{-1}, 200 μg mL^{-1} and 250 μg mL^{-1} were obtained with the mobile phase as a solvent. Under the flow rate of 1.0 mL min^{-1}, the column temperature of 30 °C and the injection volume of 10 μL, the peak area was detected at 308 nm. The linear regression equation of WF was obtained by a linear regression.

C60–Fe_3O_4 loaded with warfarin: 15 mg C60–Fe_3O_4 and 22.5 mg WF were also placed in a distilled water. After stirring at 40 °C for 4 h, C60–Fe_3O_4–WF complex was obtained after filtration and drying.

1.3 Preparation of PLA–Tween composited drug-loading C60–Fe_3O_4 microbubbles

0.3 g PLA was completely dissolved in 10 mL dichloromethane, then 1 mL Tween was added. 0.30 mL DOX–C60–Fe_3O_4, NET–C60–Fe_3O_4 and WF–C60–Fe_3O_4 complex suspension with a concentration of 0.6 g mL^{-1} was respectively dropped into above system, ultrasonic emulsification was performed for 5 min under N_2 and a primary emulsion was formed. Primary emulsion was dropped into 50 mL PVA solution with a concentration of 1%, after secondary ultrasonic emulsification was sustained for 5 min, and secondary emulsion was obtained. And 60 mL isopropanol aqueous solution (5%) was added to the secondary emulsion, the magnetic stirring was employed for 4 h in order to evaporate dichloromethane. The whole system was repeatedly centrifuged with the double distilled water and its lower layer was collected and then lyophilized. PLA–Tween-composited C60–Fe_3O_4–DOX microbubbles, PLA–Tween-composited C60–Fe_3O_4–NET microbubbles and PLA–Tween-composited C60–Fe_3O_4–WF microbubbles were obtained, respectively. Microbubbles size and Zeta potential were measured by laser particle size analyzer, and its morphology was observed by scanning electron microscope.

1.4 Determination of drug content in PLA–Tween composited C60–Fe_3O_4 microbubbles

10 mg freeze-dried powders of PLA–Tween composited C60–Fe_3O_4–DOX microbubbles were dispersed in an appropriate amount of anhydrated ethanol. Drug was released for 2 h under ultrasonic condition. Microporous membrane filtration was

conducted and the obtained filtrate was fixed to 20 mL. DOX loading rate in the composite microbubbles was calculated according to the DOX standard curve.

10 mg freeze-dried powders of PLA–Tween composited C60–Fe_3O_4–NET microbubbles were dispersed in an appropriate amount of mobile phase (pH = 2.2 potassium dihydrogen phosphate : acetonitrile = 75 : 25), ultrasonic drug release was sustained for 2 h, the drug release system was filtered and the obtained filtrate was fixed to 20 mL. The peak area of the filtrate was measured at 205 nm by HPLC. NET loading rate in the composite microbubbles was calculated according to NET standard curve.

10 mg freeze-dried powders of PLA–Tween composited C60–Fe_3O_4–WF microbubbles were dispersed in an appropriate amount of mobile phase (acetonitrile : water : glacial acetic acid = 70 : 30 : 1). After ultrasonic drug release of 2 h, filtration was carried out through a microporous membrane and the filtrate volume was constant to 20 mL. The peak area of the filtrate at 308 nm was determined by HPLC. The WF loading rate in the composite microbubbles was calculated according to the standard curve of WF.

1.5 Ultrasound imaging effect of PLA–Tween composited C60–Fe_3O_4 microbubbles

In the ultrasound imaging experiment *in vitro* and *vivo*, different microbubbles group was prepared as a suspension of 40 mg mL^{-1} with the degassed normal saline. All animal procedures were performed in accordance with the Guidelines for Care and Use of Laboratory Animals of Jiamusi University, China and approved by the Biological and Medical Ethics Committee, Jiamusi University, China (No. JMSU-233).

1.5.1 *In vitro* ultrasound of PLA–Tween composited C60–Fe_3O_4 microbubbles. Silicone tube was put into the water tank with a sponge silencing layer at the bottom, both ends of the silicone tube were set outside the liquid level and the outlet was upward. Normal saline, PLA–Tween microbubbles suspension and PLA–Tween composited C60–Fe_3O_4 microbubbles suspension were injected from one end of the silicone tube and their ultrasonic effects were tested by a doppler color ultrasound diagnostic instrument, respectively.

1.5.2 Ultrasonic imaging of rabbit kidney for PLA–Tween composited C60–Fe_3O_4–DOX microbubbles. A New Zealand white rabbit of 2 kg was respectively injected with normal saline, PLA–Tween microbubbles suspension and PLA–Tween composited C60–Fe_3O_4–DOX microbubbles suspension at a dose of 0.5 mL kg^{-1} and no greater than 2.5 mL. Under the external magnetic field, the targeted ultrasonic imaging effect of PLA–Tween composited C60–Fe_3O_4–DOX microbubbles was detected.

1.5.3 Ultrasonic imaging of rabbit bladder for PLA–Tween composited C60–Fe_3O_4–NET microbubbles. At a dose of 0.5 mL $kg^{-1}$and not higher than 2.5 mL, New Zealand white rabbit was perfused with normal saline, PLA–Tween microbubbles suspension and PLA–Tween composited C60–Fe_3O_4–NET microbubbles suspension through a bladder intubation. The ultrasonic imaging effect on the rabbit bladder for different group was observed with or without a magnetic field.

1.5.4 Ultrasonic imaging of rabbit abdominal aorta for PLA–Tween composited C60–Fe_3O_4–WF microbubbles. New Zealand white rabbit was anesthetised and its abdominal cavity was opened. The abdominal aorta was dissected and the blood vessel of 1 cm was preserved by ligation with a surgical thread. Filter paper soaked with $FeCl_3$ was covered on the blood vessel for 15 min, the ligation line was untied and the rabbit was sutured.

New Zealand white rabbit was respectively injected with normal saline, PLA–Tween microbubbles suspension and PLA–Tween composited C60–Fe_3O_4–WF microbubbles suspension through the auricular vein. Ultrasonic imaging effect of different sample on the rabbit abdominal aorta was observed. Under the additional magnetic field, the targeted ultrasonic imaging effect of PLA–Tween composited C60–Fe_3O_4–WF microbubbles was measured.

1.6 Adjuvant therapy effects of PLA–Tween composited drug-loading C60–Fe_3O_4 microbubbles

1.6.1 *In vitro* anti-tumor activity of PLA–Tween composited C60–Fe_3O_4–DOX microbubbles

1.6.1.1 In vitro anti-tumor activity of composite microbubbles with different concentration by CCK-8 method. First, the suspension of breast cancer MDA-MB-231 cells was diluted to 1×10^4 cells per 100 μL, and inoculated into 96-well plates. Suspension solutions of PLA–Tween composited C60–Fe_3O_4–DOX microbubbles with the concentration of 2.5, 5, 10, 20 and 40 mg mL^{-1} were respectively prepared with fresh DMEM culture medium, and then transferred into 96-well plate at 100 μL per well. Six auxiliary wells were set for each concentration. After culture for 12 h, 24 h and 48 h, the drug-containing culture medium was sucked out, each hole was washed with PBS for 2–3 times and 100 μL CCK8 dilution was added (CCK8 : DMEM culture medium = 1 : 9), cells were incubated at 37 °C, 5% CO_2 and completely saturated humidity for 1 h. The absorbance of each well at 450 nm was detected by the enzyme plate analyzer. The inhibition rate of cell growth was calculated according to the formula.

$$\text{Cell inhibition rate} = \frac{\text{OD value of control group-OD value of experimental group}}{\text{OD value of control group-OD value of blank group}}$$

1.6.1.2 In vitro anti-tumor activity of different composite microbubbles by CCK-8 method. DMEM culture medium was set as the control group, and PLA–Tween composited C60–Fe_3O_4–DOX microbubbles, PLA–Tween composited C60–DOX microbubbles, PLA–Tween microbubbles and free DOX were set as the experimental groups. With DMEM as the solvent, every microbubbles group was prepared into a suspension of 13.2 mg mL^{-1}, and DOX was prepared a solution with a concentration of 0.74 mg mL^{-1}. Each group was provided with three accessory pores and interacted with breast cancer MDA-MB-231 cells. The

inhibitory effect of different composite microbubbles on MDA-MB-231 cells was detected by CCK8 method, and the cell status was observed under a microscope.

1.6.1.3 Toxicity of different composite microbubbles on normal mouse fibroblasts 3T3 cells. Experimental grouping and procedures were the same as 2.6.1.2. CCK8 method was used to detect the effect of every composite microbubbles group on the growth of normal mouse fibroblasts 3T3 cells, and the cell status was observed under a microscope.

1.6.2 *In vitro* bacteriostatic activity of PLA–Tween composited C60–Fe_3O_4–NET microbubbles

1.6.2.1 Composite microbubbles with different concentration. Drug sensitive papers of PLA–Tween composited C60–Fe_3O_4–NET microbubbles suspension with the concentration of 0 mg mL^{-1}, 10 mg mL^{-1}, 20 mg mL^{-1}, 40 mg mL^{-1}, 60 mg mL^{-1}, and 80 mg mL^{-1} were covered on the AGAR plate surface of *Escherichia coli* and *Staphylococcus aureus*, respectively. Three parallel samples were conducted for each concentration. After culture of 24 h in a 37 °C incubator, the AGAR plates were taken out, the antibacterial effects of the composite microbubbles were evaluated with the antibacterial circle diameter as an index.

1.6.2.2 Different composite microbubbles. Drug-sensitive papers of PLA–Tween microbubbles, PLA–Tween composited C60–Fe_3O_4 microbubbles, PLA–Tween composited C60–NET microbubbles and PLA–Tween composited C60–Fe_3O_4–NET microbubbles were covered on the surface of *Escherichia coli* plate and *Staphylococcus aureus* plate, respectively. Three parallel samples were conducted for each group. All samples were cultured in a 37 °C constant temperature incubator for 24 h and then taken out for observation.

1.6.3 *In vitro* antithrombotic activity of PLA–Tween composited C60–Fe_3O_4–WF microbubbles

1.6.3.1 In vitro antithrombotic of composite microbubbles with different concentration. Suspensions of PLA–Tween composited C60–Fe_3O_4–WF microbubbles with concentrations of 0 mg mL^{-1}, 10 mg mL^{-1}, 20 mg mL^{-1}, 40 mg mL^{-1}, 60 mg mL^{-1} and 80 mg mL^{-1} were prepared and broken under the ultrasound. Blood samples were taken from the ear vein of New Zealand white rabbits and acted with the suspensions of different composite microbubbles, respectively. The wet and dry weight of thrombus were recorded. Three parallel tests were conducted for each concentration.

1.6.3.2 In vitro antithrombotic of different composite microbubbles. Suspensions of PLA–Tween microbubbles, PLA–Tween composited C60–WF microbubbles, PLA–Tween composited C60–Fe_3O_4–WF with a concentration of 80 mg L^{-1} were prepared and broken under the ultrasound. Blood samples of New Zealand white rabbits interacted with normal saline and different microbubbles suspensions, respectively. After 1 h, the wet and dry weight of the clot were recorded. Three parallel experiments were conducted for each sample.

1.6.3.3 In vitro anticoagulation of composite microbubbles with different concentration. Suspensions of PLA–Tween composited C60–Fe_3O_4–WF microbubbles with concentrations of 0 mg mL^{-1}, 10 mg mL^{-1}, 20 mg mL^{-1}, 40 mg mL^{-1}, 60 mg mL^{-1} and 80 mg mL^{-1} were prepared and broken under the ultrasound. After composite microbubbles with different concentration were reacted with blood samples of New Zealand white rabbits, prothrombin time (PT), activated partial thromboplastin time (APTT) and thrombin time (TT) were measured by automatic blood coagulation analyzer.

1.6.3.4 In vitro anticoagulation of different composite microbubbles. Suspensions of PLA–Tween, PLA–Tween composited C60–WF and PLA–Tween composited C60–Fe_3O_4–WF microbubbles with a concentration of 80 mg L^{-1} were prepared and broken under the ultrasound. After physiological saline and different composite microbubbles were reacted with blood samples of New Zealand white rabbits, prothrombin time (PT), activated partial thromboplastin time (APTT) and thrombin time (TT) were measured by automatic blood coagulation analyzer.

2 Results and discussions

SEM and TEM of PLA–Tween composited C60–Fe_3O_4 microbubbles are shown in Fig. 1. From Fig. 1, PLA–Tween composited C60–Fe_3O_4 microbubble was hollow structure with N_2 inside. The obtained composite microbubbles had a nanoscale in size, smooth surface, uniform particle size, regular sphere and full shape. In the preparation process, Fe_3O_4 and C60 formed C60–Fe_3O_4 magnetically targeted complex through *in*

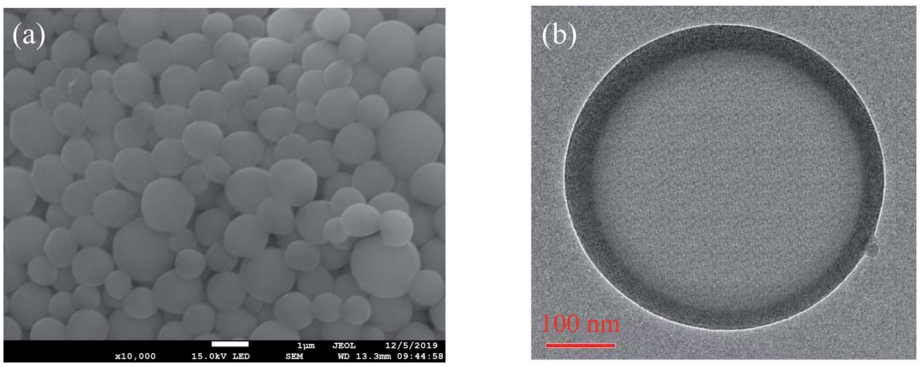

Fig. 1 SEM (a) and TEM (b) of PLA–Tween composited C60–Fe_3O_4 microbubbles.

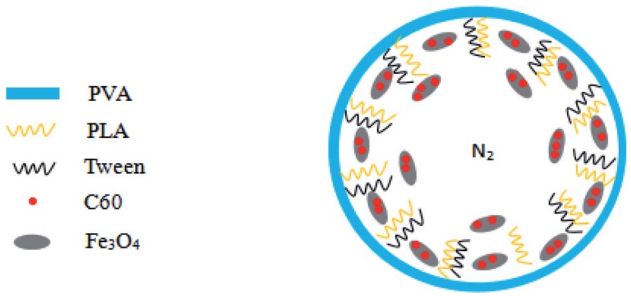

Fig. 2 The structure simulation diagram of PLA–Tween composited C60–Fe_3O_4 microbubbles.

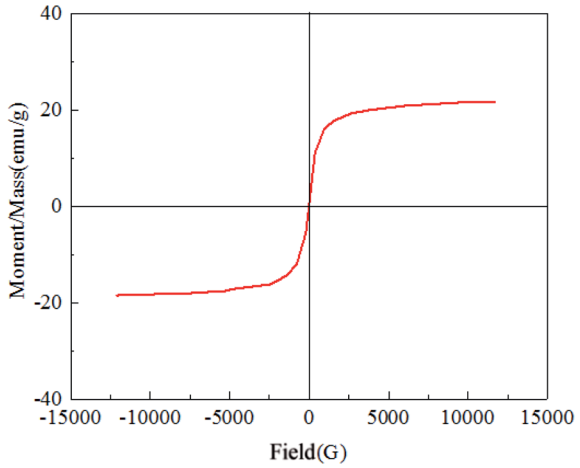

Fig. 3 Hysteresis curve of PLA–Tween composited C60–Fe_3O_4 microbubbles.

situ deposition, and the obtained C60–Fe_3O_4 complex solution was transferred to dichloromethane solution of PLA and Tween. Under the first ultrasound, PLA and Tween were dispersed and broken, and C60–Fe_3O_4 complex was wrapped by PLA and Tween to form a primary emulsion. During the process of microbubbles forming, Tween molecules were interspersed into PLA molecules, the hydrophilic end of Tween was inward and its oil-philic end was outward, the stable microbubbles were formed. Primary emulsion was transferred to the PVA solution for a second ultrasonic emulsification. As a stabilizer of the external water phase, PVA will gather and wrap on the surface of PLA–Tween microbubble to form a shell layer under the ultrasound, a multiple emulsion formed. The multiple emulsion was transferred into the isopropanol solution, stirring for a certain time, the dichloromethane solvent evaporated. After freeze-drying, C60–Fe_3O_4 complex adhered to the interlayer and inner of the microbubbles, as shown in the shadow part in Fig. 1(b). Structure simulation diagram of PLA–Tween composited C60–Fe_3O_4 microbubble is shown in Fig. 2.

Fig. 3 shows the hysteresis curve of PLA–Tween composited C60–Fe_3O_4 microbubbles. It can be seen that there was no coercive magnetic field and remanence at the zero point, indicating that the obtained composite microbubbles had good magnetism. Fig. 4 shows the particle size distribution (Fig. 4(a)) and Zeta potential (Fig. 4(b)) of PLA–Tween composited C60–Fe_3O_4 microbubbles. The obtained composite microbubbles had a uniform and unimodal distribution size, and an average particle size of 446.4 nm. Zeta potential of the composite microbubble was −40.5 mV, which indicated that PLA–Tween composited C60–Fe_3O_4 microbubbles had good stability.

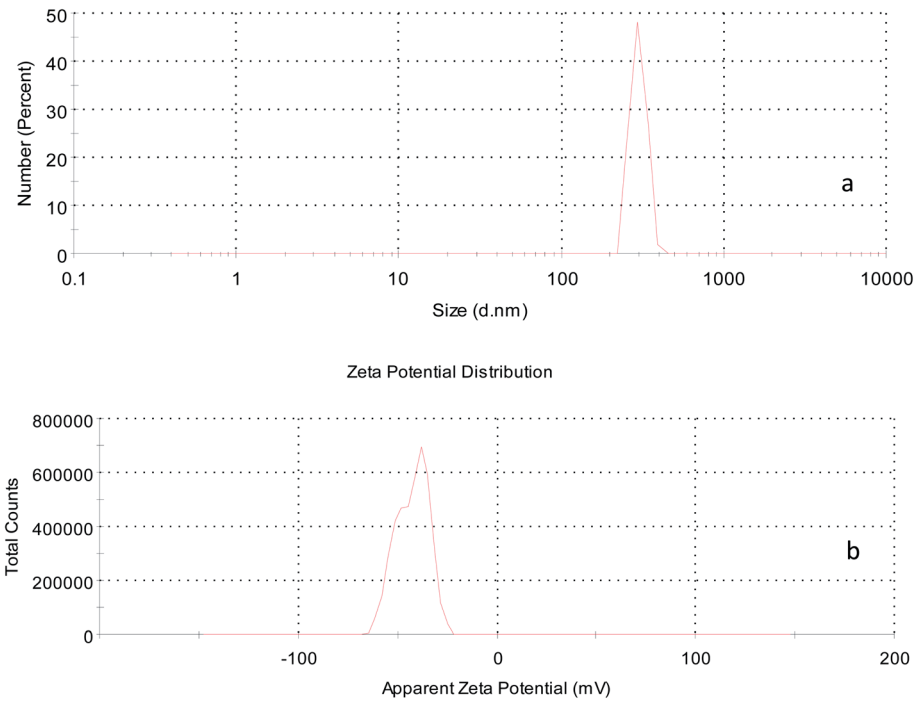

Fig. 4 Size (a) and Zeta potential (b) of PLA–Tween composited Fe_3O_4–C60 microbubbles.

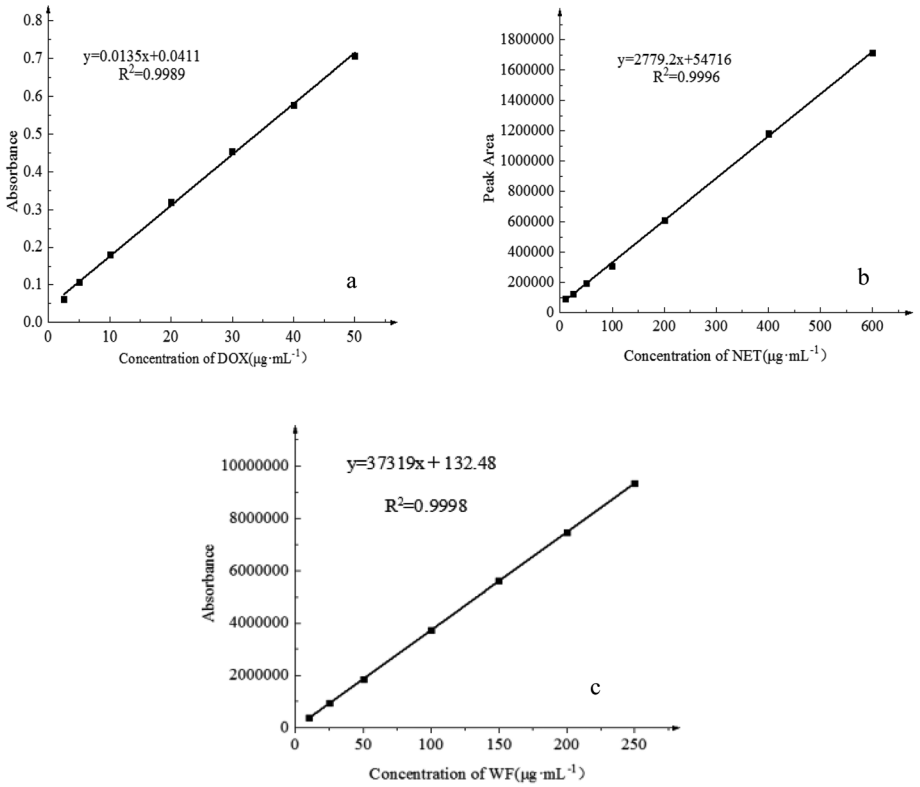

Fig. 5 Standard curve of DOX (a), NET (b) and WF (c).

Table 1 Drug loading rate in the composite microbubble ($n = 5$)

Experiment number	1	2	3	4	5	Average
Loading rate of DOX (%)	5.38	6.07	5.52	5.19	5.71	5.58
Loading rate of NET (%)	7.50	8.25	8.99	7.31	8.68	8.15
Loading rate of WF (%)	2.89	3.06	3.77	3.52	3.60	3.37

The standard curves of DOX, NET and WF are shown in Fig. 5. Equation of DOX standard curve was $y = 0.0135x + 0.0411$ ($R^2 = 0.9989$), DOX concentration had a good linear relationship with the absorbance in the range of 2.5–50 μg mL^{-1}. $y = 2779.2x + 54\,716$ ($R^2 = 0.9996$) was a equation of NET standard curve. In the range of 10–600 μg mL^{-1}, the concentration of NET had a good linear relationship with the peak area. The standard curve equation of WF was $y = 373\ 19x + 132.48$ ($R^2 = 0.9998$). In the range of 10–250 μg mL^{-1}, the WF concentration had a good linear relationship with the peak area.

Drug loading rates in PLA–Tween composited drug-loading C60–Fe_3O_4 microbubbles are shown in Table 1. The loading rate of DOX in PLA–Tween composited C60–Fe_3O_4–DOX microbubbles was 5.58%, the loading rate of NET in PLA–Tween composited C60–Fe_3O_4–NET microbubbles was 8.15%, and the loading rate of WF in PLA–Tween composited C60–Fe_3O_4–WF microbubbles was 3.37%, respectively.

In vitro ultrasonic imaging effects of the normal saline group, PLA–Tween microbubbles group and PLA–Tween composited C60–Fe_3O_4 microbubbles group were shown in Fig. 6. For normal saline group (Fig. 6(a)), the echo was low and the imaging of silicone tube was blurred. For PLA–Tween microbubble group (Fig. 6(b)), the ultrasonic signal in the silicone tube was enhanced, the visual field was brightened and the ultrasonic effect was significantly improved. After injection of PLA–Tween composited C60–Fe_3O_4 microbubbles group (Fig. 6(c)), the field of vision was clear and bright, and the silicone tube profile was clear. Therefore, both PLA–Tween microbubbles and PLA–Tween composited C60–Fe_3O_4 microbubbles had good ultrasonic imaging effect *in vitro*.

Ultrasonic imaging effects of rabbit kidney for normal saline group, PLA–Tween microbubbles group, PLA–Tween composited C60–Fe_3O_4–DOX microbubbles group with or without external magnetic field are shown in Fig. 7. As can be seen from Fig. 7(a), the imaging field of normal saline group was dark, and the blood echo was low, as a result, the effective imaging cannot be performed and the lesion could not be observed clearly. For PLA–Tween microbubbles group and PLA–Tween composited C60–Fe_3O_4–DOX microbubbles group (Fig. 7(b) and (c)), the signal rapidly enhanced and the picture significantly brighter, which could achieve a effective development. After the external magnetic field was applied, as shown in Fig. 7(d), the ultrasonic signal intensity of PLA–Tween composited C60–Fe_3O_4–DOX microbubbles was significantly enhanced, which indicated that the PLA–Tween composited C60–Fe_3O_4–DOX microbubbles can be effectively enriched in the magnetic field region, thus the targeted imaging was realized. At the same time, the ultrasonic

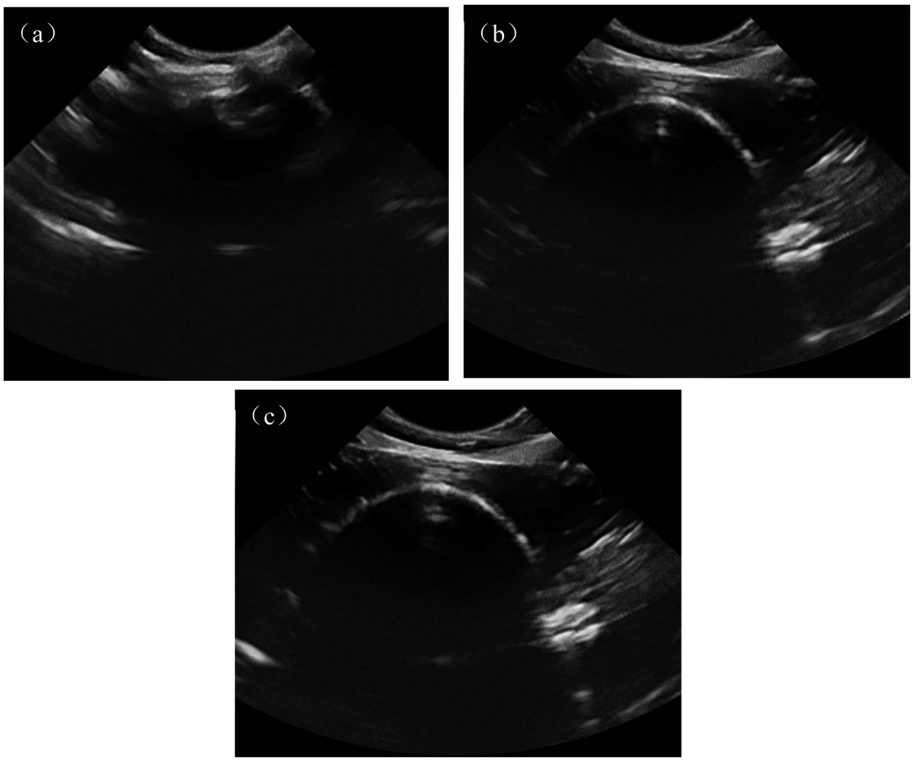

Fig. 6 *In vitro* ultrasound images of different sample (a) saline group (b) PLA–Tween microbubbles group (c) PLA–Tween composited C60–Fe_3O_4 microbubbles group.

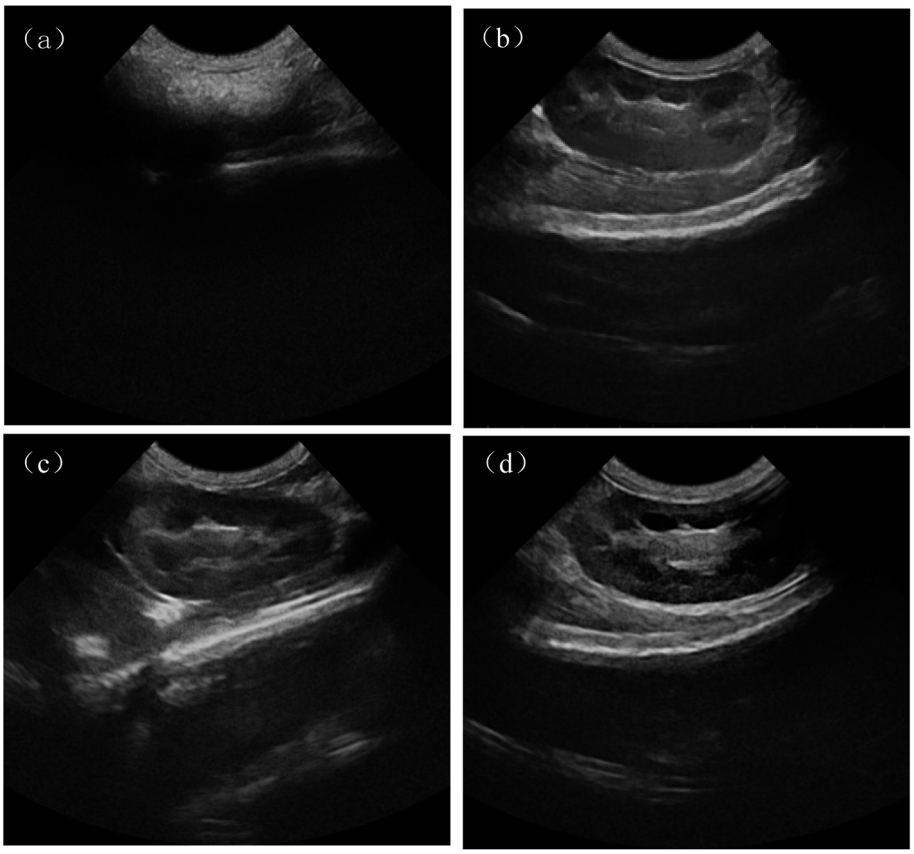

Fig. 7 Ultrasonic images of rabbit kidney after the injection of different sample (a) saline group (b) PLA–Tween microbubbles group (c) PLA–Tween composited C60–Fe_3O_4–DOX microbubbles group (d) PLA–Tween composited C60–Fe_3O_4–DOX microbubbles under additional magnetic field group.

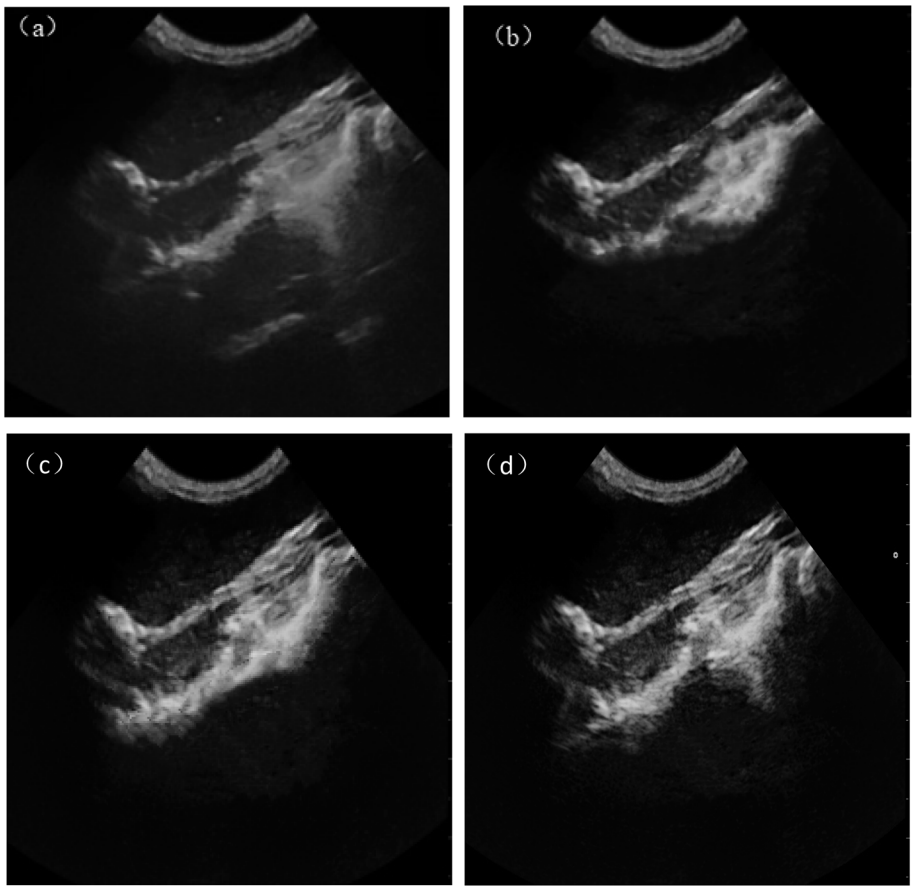

Fig. 8 Ultrasonic images of rabbit bladder after the injection of different sample (a) saline group (b) PLA–Tween microbubbles group (c) PLA–Tween composited C60–Fe_3O_4–NET microbubbles group (d) PLA–Tween composited C60–Fe_3O_4–NET microbubbles under additional magnetic field.

development effect and ultrasonic development time under the additional magnetic field were significantly improved.

Fig. 8 is ultrasonic images of rabbit bladder for normal saline group, PLA–Tween microbubbles group, PLA–Tween composited C60–Fe_3O_4–NET microbubbles with and without a external magnetic field. As can be seen from Fig. 8(a), the imaging vision of normal saline group was dark and the blood echo was low, so lesion could not be observed effectively. After infusing PLA–Tween microbubbles group and PLA–Tween composited with C60–Fe_3O_4–NET microbubbles group (Fig. 8(b) and (c)), the pictures became significantly brighter and the echo were significantly enhanced, as a result, the effective development could be achieved. After the external magnetic field was applied as shown in Fig. 8(d), the ultrasonic signal intensity in this region for PLA–Tween composited C60–Fe_3O_4–NET microbubbles group was significantly enhanced, the vision field was brighter, and the organ imaging was clearer, which indicated that PLA–Tween composited with C60–Fe_3O_4–NET microbubbles could achieve a good targeted ultrasonic imaging effect in the external magnetic field. Ultrasonic images of rabbit abdominal aorta for the normal saline group, PLA–Tween microbubbles group and PLA–Tween composited C60–Fe_3O_4–WF microbubbles group are shown in Fig. 9. From Fig. 9(a), the contrast field of normal saline group was dark, and the outline of rabbit abdominal aorta could not be seen clearly, so it could not effectively be observed. After PLA–Tween microbubbles and PLA–Tween composited C60–Fe_3O_4–WF microbubbles were injected respectively, the abdominal aorta vessel rapidly filled, the signal was enhanced and the picture was significantly brighter, as shown in Fig. 9(b) and (c). After addition of the external magnetic field, the ultrasonic signal intensity of PLA–Tween composited C60–Fe_3O_4–WF microbubbles group was significantly enhanced, as shown in Fig. 9(d), the picture became filled and brighter, and it was clearer than that without the external magnetic field, indicating that PLA–Tween composited C60–Fe_3O_4–WF microbubbles could be effectively enriched in the magnetic field area, thus the development effect improved.

Table 2 is the inhibitory effect of PLA–Tween composited C60–Fe_3O_4–DOX microbubbles with different concentration on the breast cancer MDA-MB-231 cells. From Table 2, the inhibition rate increased with the increase of the concentration and action time of the composite microbubbles, indicating that PLA–Tween composited with C60–Fe_3O_4–DOX microbubbles could inhibit the growth of breast cancer MDA-MB-231 cells. According to SPSS22.0 statistical software analysis, the IC50

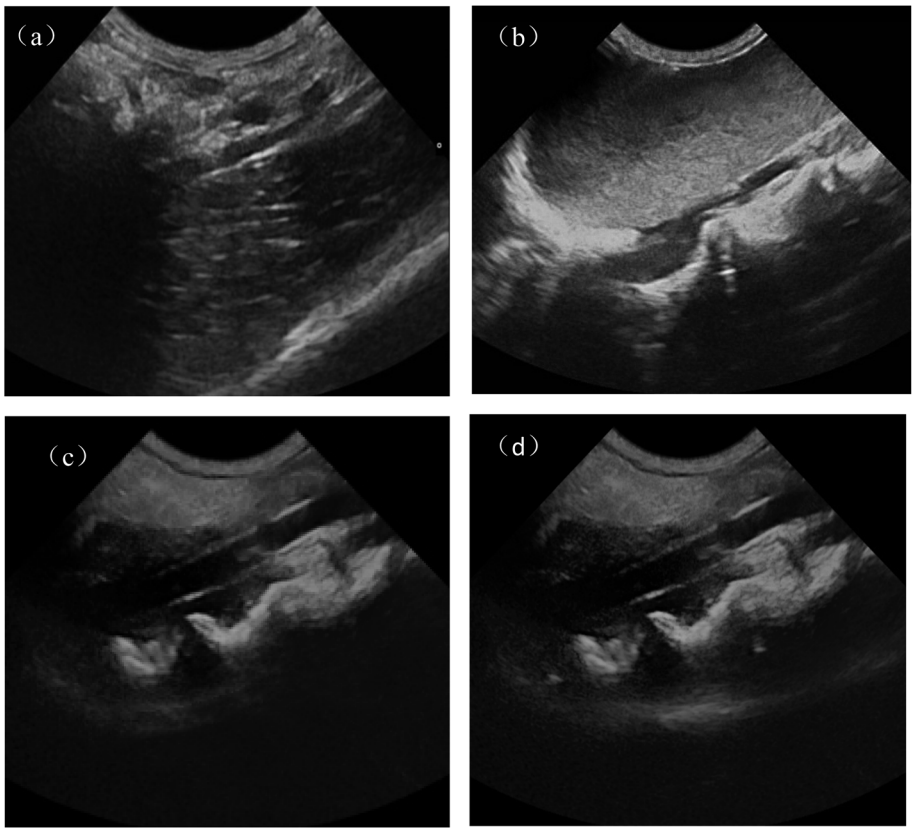

Fig. 9 Ultrasonic images of rabbit abdominal aorta after the injection of different contrast agent (a) saline group (b) PLA–Tween microbubbles (c) PLA–Tween composited C60–Fe_3O_4–WF microbubbles group (d) PLA–Tween composited C60–Fe_3O_4–WF microbubbles under additional magnetic field.

values at 12 h, 24 h and 48 h were 41.331 mg mL^{-1}, 13.201 mg mL^{-1} and 6.353 mg mL^{-1}, respectively. IC50 value of 48 h was too small and easy to produce error, while IC50 value of 12 h was too large, and the drug could not completely interact with the cells. So 24 h was selected as a suitable action time on the breast cancer MDA-MB-231 cells. The inhibitory rates of different composite microbubbles on the breast cancer MDA-MB-231 cells are shown in Fig. 10. Inhibition rates of PLA–Tween microbubbles, PLA–Tween composited C60–DOX microbubbles, PLA–Tween composited Fe_3O_4–C60–DOX microbubbles and free DOX on MDA-MB-231 cells were 13.2 ± 1.9%, 56.8 ± 0.7%, 53.4 ± 1.3%, 69.4 ± 3.2%, respectively. As can be seen from Fig. 10, after free DOX, PLA–Tween microbubbles, PLA–Tween composited Fe_3O_4–C60–DOX

Table 2 Inhibition rates of PLA–Tween composited C60–Fe_3O_4–DOX microbubbles with different concentration on the breast cancer MDA-MB-231 cells ($\bar{x} \pm s$)

Concentration of composite microbubbles (mg mL^{-1})	Inhibition rate (%)		
	12 h	24 h	48 h
0	0	0	0
2.5	16.5 ± 0.5	28.7 ± 1.2	34.3 ± 0.4
5	21.4 ± 1.1	35.2 ± 0.7	47.7 ± 0.6
10	28.4 ± 0.3	40.6 ± 0.1	58.1 ± 1.5
20	40.3 ± 0.8	58.9 ± 0.9	65.5 ± 2.1
40	49.6 ± 1.3	67.1 ± 1.4	77.7 ± 1.7
IC_{50}	41.331	13.201	6.353

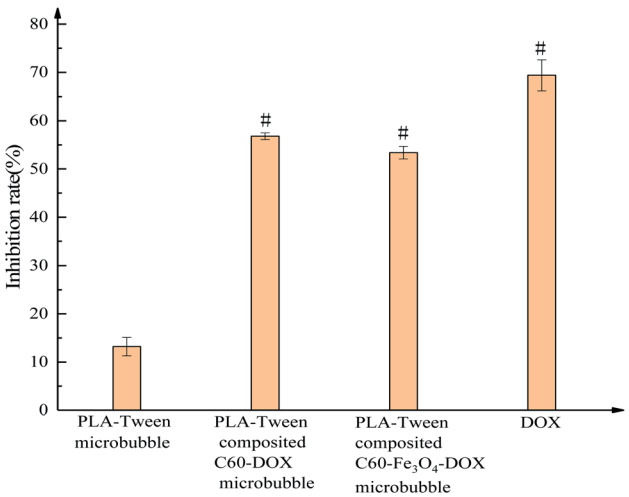

Fig. 10 Inhibition rates of different composite microbubbles on the breast cancer MDA-MB-231 cells. Note: compared to PLA–Tween microbubbles, "#" is $P < 0.01$.

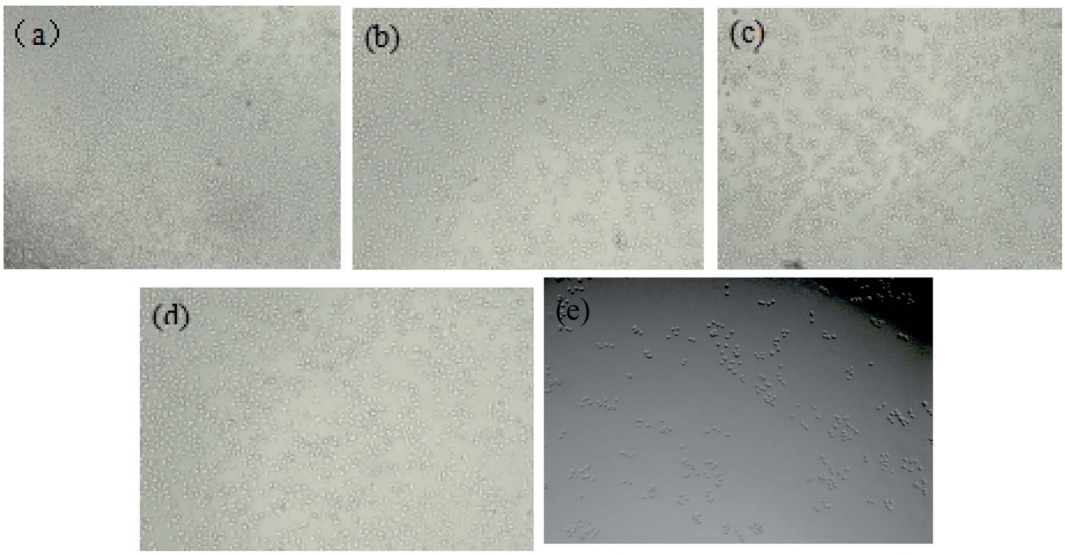

Fig. 11 Microscopic photographs of inhibition effects for different samples on the breast cancer MDA-MB-231 cell (a) no treatment control group (b) PLA–Tween microbubbles group (c) PLA–Tween composited C60–Fe_3O_4–DOX microbubbles group (d) PLA–Tween composited C60–DOX microbubbles (e) free DOX group.

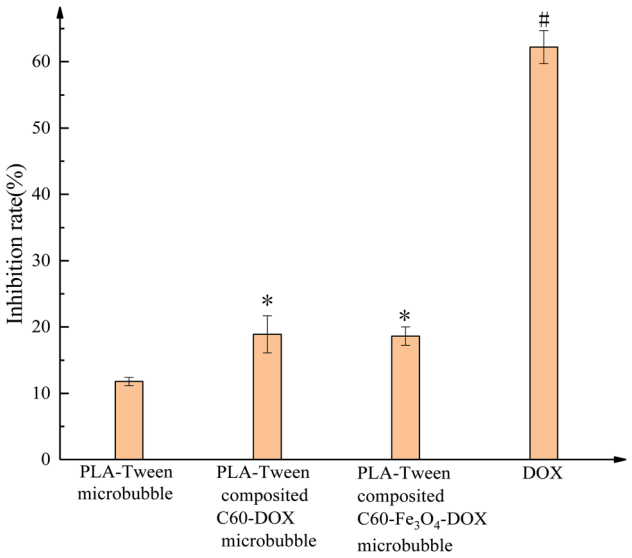

Fig. 12 Inhibition rates of different microbubbles on the normal mouse fibroblast 3T3 cells. Note: compared to PLA–Tween microbubbles,"*" is $0.01 < P < 0.05$, "#" is $P < 0.01$.

microbubbles, PLA–Tween composited C60–DOX microbubbles interacted with the breast cancer cells for 24 h, they had the inhibitory effects on MDA-MB-231 cells. Moreover, free DOX, PLA–Tween composited Fe_3O_4–C60–DOX microbubbles, PLA–Tween composited C60–DOX microbubbles had significant differences ($P < 0.01$) in comparison with PLA–Tween microbubbles. Microscopic photographs (Fig. 11) also showed that the control group had more cell number and higher cell density. There was no significant difference between PLA–Tween microbubbles (Fig. 11(b)) and the control group (Fig. 11(a)), indicating that PLA–Tween membrane material had no significant inhibitory effect on the breast cancer MDA-MB-231 cells. Cell density significantly decreased for PLA–Tween composited Fe_3O_4–C60–DOX microbubbles group (Fig. 11(c)) and PLA–Tween composited C60–DOX microbubbles group (Fig. 11(d)), which indicated that both had inhibitory effect on the growth of breast cancer MDA-MB-231 cells. While the cell density of free DOX group (Fig. 11(e)) was the lowest, and its inhibitory effect on breast cancer cells was the most obvious and the toxicity was the strongest. It is worth noting that there was no significant difference for the inhibitory effects of PLA–Tween composited C60–DOX microbubbles and PLA–Tween composited Fe_3O_4–C60–DOX on the breast cancer MDA-MB-231 cells, indicating that Fe_3O_4 in PLA–Tween composited Fe_3O_4–C60–DOX microbubbles did not affect its pharmacological effect.

The inhibition rates and micrographs of different samples treated with normal mouse fibroblast 3T3 cells for 24 h are shown in Fig. 12. The inhibition rates of PLA–Tween microbubbles, PLA–Tween composited C60–DOX microbubbles, PLA–Tween composited Fe_3O_4–C60–DOX microbubbles and free DOX group on 3T3 cells growth were $11.8 \pm 0.6\%$, $18.9 \pm 2.8\%$, $18.6 \pm 1.4\%$ and $62.2 \pm 2.5\%$, respectively. Compared with PLA–Tween microbubbles, PLA–Tween composited C60–DOX microbubbles and PLA–Tween composited Fe_3O_4–C60–DOX were significantly difference ($0.01 < P < 0.05$), and free DOX was significantly difference ($P < 0.01$). As can be seen from Fig. 13, the cell density of free DOX group was much lower than that of PLA–Tween microbubbles, PLA–Tween composited C60–Fe_3O_4–DOX microbubbles, and PLA–Tween composited C60–DOX microbubbles. That is, the toxicities of PLA–Tween microbubbles, PLA–Tween composited C60–Fe_3O_4–DOX microbubbles and PLA–Tween composited C60–DOX microbubbles on normal mouse fibroblast 3T3 cells were far lower than that of free DOX, which indicated that free DOX could not only

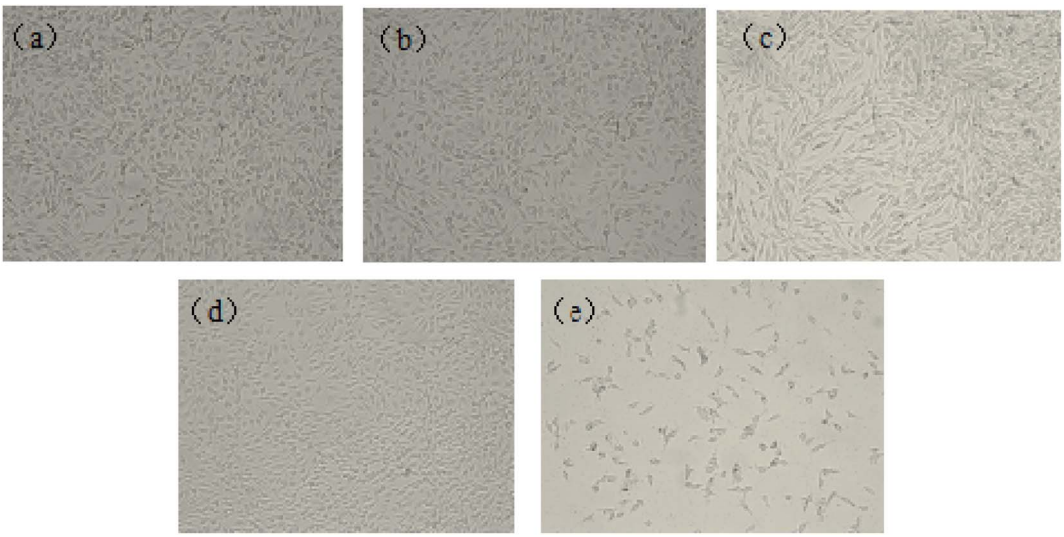

Fig. 13 Inhibition microscopic photographs of different sample on the normal mouse fibroblast 3T3 cells (a) no treatment control group (b) PLA–Tween microbubbles group (c) PLA–Tween composited C60–Fe_3O_4–DOX microbubbles group (d) PLA–Tween composited C60–DOX microbubbles group (e) free DOX group.

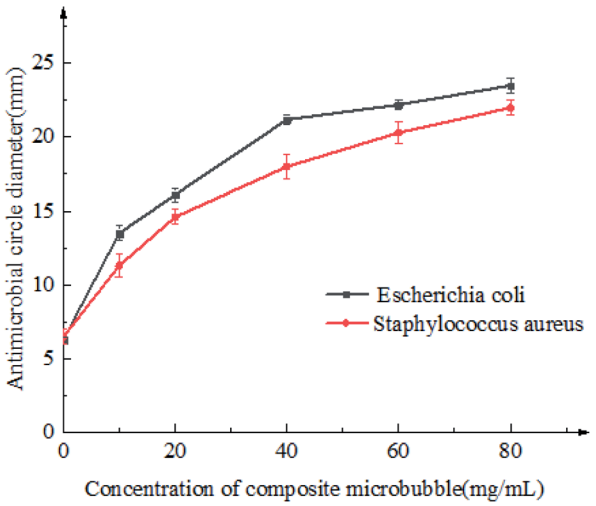

Fig. 14 Inhibition curves of PLA–Tween composited C60–Fe_3O_4–NET microbubbles with different concentration on *Escherichia coli* and *Staphylococcus aureus*.

significantly inhibit the growth of the breast cancer MDA-MB-231 cells but also cause too much damage on the normal cells. For PLA–Tween composited C60–Fe_3O_4–DOX microbubbles, DOX was loaded on C60 and coated in PLA–Tween membrane material during the preparation, which significantly reduced the toxicity of DOX on the normal cells, and also inhibited the growth of the breast cancer cells.

Inhibitory effects of PLA–Tween composited C60–Fe_3O_4–NET microbubbles with the different concentration on *Escherichia coli* and *Staphylococcus aureus* were shown in Fig. 14 and 15. As can be seen from Fig. 14 and 15, the bacteriostatic effect was gradually enhanced with the increase of the concentration of PLA–Tween composited C60–Fe_3O_4–NET microbubbles. The diameters of inhibitory zone of PLA–Tween composited C60–Fe_3O_4–NET microbubbles with the different concentration on *Escherichia coli* and *Staphylococcus aureus* are shown in Table 3. For *Escherichia coli*, the inhibition zone diameter was 6.3 ± 0.2 mm when the concentration of PLA–Tween composited C60–Fe_3O_4–NET microbubbles was 0 mg mL^{-1}. The composite microbubbles concentration was from 10 mg mL^{-1} to 80 mg mL^{-1}, the inhibition zone diameter had a very significant difference in comparison with that of 0 mg mL^{-1} ($P < 0.01$). Specifically, the inhibition zone diameter was 13.50 ± 0.50 mm when the composite microbubbles concentration was 10 mg mL^{-1}, and the drug sensitivity was medium sensitive. When the composite microbubbles concentration was 20 mg mL^{-1}, the inhibition zone diameter was 16.10 ± 0.46 mm, and the drug sensitivity was highly sensitive. When the composite microbubbles concentration was 40–80 mg mL^{-1}, the diameter of the inhibition zone was 21.2 ± 0.3 mm to 23.50 ± 0.5 mm, indicating that the drug sensitivity was extremely sensitive. For *Staphylococcus aureus*, the inhibition zone diameter was 6.5 ± 0.5 mm when the concentration of PLA–Tween composited C60–Fe_3O_4–NET microbubbles was 0 mg mL^{-1}. When the composite microbubbles concentration was from 10 mg mL^{-1} to 80 mg mL^{-1}, the inhibition zone diameter had a very significant difference in comparison with that of 0 mg mL^{-1} ($P < 0.01$); when the concentration of PLA–Tween composited C60–Fe_3O_4–NET microbubbles was 10–20 mg mL^{-1}, the diameter of the inhibition zone was 11.30 ± 0.75 mm to 14.60 ± 0.50 mm, and the drug sensitivity was medium sensitive. When the composite microbubbles concentration was 40 mg mL^{-1}, the inhibition zone diameter was 18 ± 0.8 mm, and the drug sensitivity was highly sensitive. When the composite microbubble concentration was greater than 60 mg mL^{-1}, the drug sensitivity was extremely sensitive. In a word, PLA–Tween composited C60–Fe_3O_4–NET microbubbles had a good

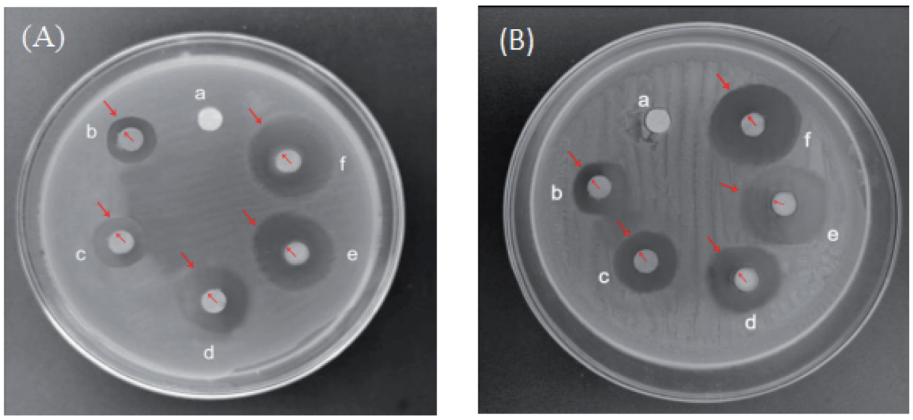

Fig. 15 Inhibition zones of PLA–Tween composited C60–Fe_3O_4–NET microbubbles with different concentration on *Escherichia coli* (A) and *Staphylococcus aureus* (B). (a) 0 mg mL^{-1} (b) 10 mg mL^{-1} (c) 20 mg mL^{-1} (d) 40 mg mL^{-1} (e) 60 mg mL^{-1} (f) 80 mg mL^{-1}.

Table 3 Inhibition zone diameters of PLA–Tween composited C60–Fe_3O_4–NET microbubbles with different concentration on *Escherichia coli* and *Staphylococcus aureus*[a]

Concentration of microbubbles (mg mL^{-1})	0	10	20	40	60	80
Diameter of inhibitory zone on *Escherichia coli*	6.30 ± 0.20	$13.50 \pm 0.50^{\#}$	$16.10 \pm 0.46^{\#}$	$21.2 \pm 0.30^{\#}$	$22.2 \pm 0.3^{\#}$	$23.50 \pm 0.5^{\#}$
Diameter of inhibitory zone on *Staphylococcus aureus*	6.50 ± 0.50	$11.30 \pm 0.75^{\#}$	$14.60 \pm 0.50^{\#}$	$18 \pm 0.8^{\#}$	$20.3 \pm 0.7^{\#}$	$22.0 \pm 0.5^{\#}$

[a] Note: compared to microbubbles of 0 mg mL^{-1}, "#" is $P < 0.01$.

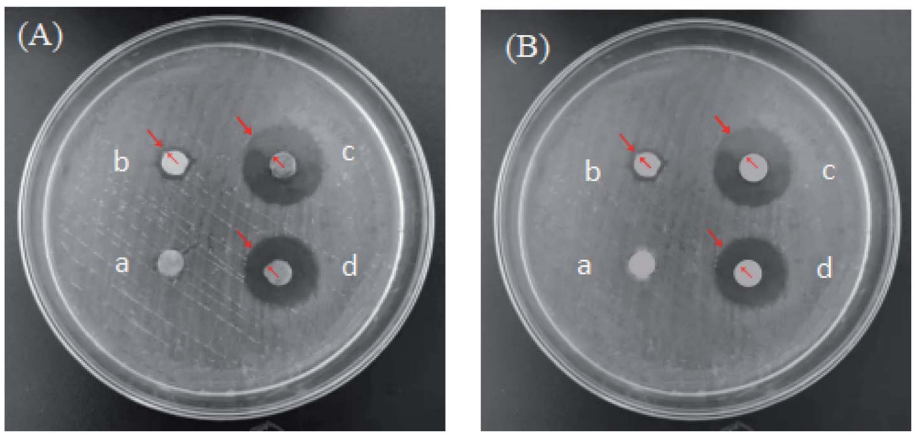

Fig. 16 Inhibition zones of different microbubbles (A) *Escherichia coli* and (B) *Staphylococcus aureus* (a) PLA–Tween microbubbles (b) PLA–Tween composited C60–Fe_3O_4 microbubbles (c) PLA–Tween composited C60–NET microbubbles (d) PLA–Tween composited C60–Fe_3O_4–NET microbubbles.

inhibitory effect on the growth of *Escherichia coli* and *Staphylococcus aureus*, and its inhibitory effect on *Escherichia coli* was better than that on *Staphylococcus aureus*.

The bacteriostatic effects of different microbubbles on *Escherichia coli* and *Staphylococcus aureus* are shown in Fig. 16. PLA–Tween microbubbles had no bacteriostatic effect, while PLA–Tween composited C60–Fe_3O_4 microbubbles had a certain bacteriostatic effect on *Escherichia coli* and *Staphylococcus aureus*, respectively. PLA–Tween composited C60–NET microbubbles and PLA–Tween composited C60–Fe_3O_4–NET microbubbles had good bacteriostatic effects on *Escherichia coli* and *Staphylococcus aureus*. The inhibition zone diameters of different microbubbles on *Escherichia coli* and *Staphylococcus aureus* are shown in Table 4. For *Escherichia coli*, the inhibition zone diameter of PLA–Tween microbubbles was 6.5 ± 0.33 mm and that of PLA–Tween composited C60–Fe_3O_4 microbubbles

Table 4 Inhibition zone diameters of different composite microbubbles on *Escherichia coli* and *Staphylococcus aureus* ($\bar{x} \pm s$)[a]

Samples	Inhibition zone diameters/mm	
	Escherichia coli	*Staphylococcus aureus*
PLA–Tween microbubbles	6.5 ± 0.33	6.6 ± 0.31
PLA–Tween composited C60–Fe_3O_4 microbubbles	8.4 ± 0.36#	8.0 ± 0.28#
PLA–Tween composited C60–NET microbubbles	18.8 ± 1.14#	18.1 ± 0.47#
PLA–Tween composited C60–Fe_3O_4–NET microbubbles	17.5 ± 0.83#	16.8 ± 0.60#

[a] Note: compared to PLA–Tween microbubbles, "#" is $P < 0.01$.

Table 5 Thrombus wet weight and dry weight of PLA–Tween composited C60–Fe_3O_4–WF microbubble at different concentrations ($\bar{x} \pm s$)[a]

No.	Concentration of composited microbubbles (mg mL^{-1})	Thrombus wet weight (mg)	Thrombus dry weight (mg)
1	0	241.13 ± 10.90	57.90 ± 6.95
2	10	236.91 ± 12.22	54.90 ± 9.54
3	20	210.20 ± 9.54*	48.30 ± 2.29
4	40	207.53 ± 13.40*	40.67 ± 6.67*
5	60	196.47 ± 11.14#	36.0 ± 4.85*
6	80	175.70 ± 9.88#	32.73 ± 5.82#

[a] Note: "*" is $0.01 < P < 0.05$, "#" is $P < 0.01$.

Table 6 Thrombus wet weight and dry weight of different composite microbubbles on thrombosis *in vitro* ($\bar{x} \pm s$)[a]

Samples	Thrombus wet weight (mg)	Thrombus dry weight (mg)
Physiological saline	241.13 ± 10.90	54.97 ± 5.04
PLA–Tween microbubbles	237.30 ± 3.99	50.27 ± 1.33
PLA–Tween composited C60–WF microbubbles	187.43 ± 6.64#	32.30 ± 5.31#
PLA–Tween composited C60–Fe_3O_4–WF microbubbles	192.97 ± 8.97#	36.00 ± 4.80*

[a] Note: compared to physiological saline group, "*" is $0.01 < P < 0.05$, "#" is $P < 0.01$.

was 8.4 ± 0.36 mm, there was a significant difference between the latter and the former ($P < 0.01$); the inhibition zone diameter of PLA–Tween composited C60–NET microbubbles were 18.8 ± 1.14 mm, it had significantly difference in comparison with PLA–Tween microbubbles group ($P < 0.01$); the inhibition zone diameter of PLA–Tween composited C60–Fe_3O_4–NET group were 17.5 ± 0.83 mm and was significantly different from PLA–Tween microbubbles group ($P < 0.01$). For *Staphylococcus aureus*, the inhibition zone diameter of PLA–Tween microbubbles group was 6.6 ± 0.31 mm, and that of PLA–Tween composited C60–Fe_3O_4 microbubble was 8.0 ± 0.28 mm, there was significantly difference for both ($P < 0.01$); the inhibition zone diameter of PLA–Tween composited C60–NET microbubbles was 18.1 ± 0.47 mm, which was significantly different from that of PLA–Tween blank microbubble group ($P < 0.01$); the inhibition zone diameter of PLA–Tween composited C60–Fe_3O_4–NET microbubbles group was 16.8 ± 0.60 mm, it had significantly difference in comparison with PLA–Tween microbubbles group ($P < 0.01$).

So, it can be concluded from above that PLA–Tween composited C60–Fe_3O_4 microbubbles, PLA–Tween composited C60–NET microbubbles and PLA–Tween composited C60–Fe_3O_4–NET have antibacterial activities on *Staphylococcus aureus* and *Escherichia coli*, this is because their bacteriostatic effect was derived from the dual action of NET and C60, and the bacteriostatic effect on *Escherichia coli* was better than that of *Staphylococcus aureus*. Moreover, there was no significant difference for the bacteriostatic effect of PLA–Tween composited C60–NET microbubbles and PLA–Tween composited C60–Fe_3O_4–NET microbubbles, indicating that Fe_3O_4 in PLA–Tween composited C60–Fe_3O_4–NET microbubbles had no significant effect on the bacteriostatic performance of the composite microbubbles.

Inhibition results *in vitro* of PLA–Tween composited Fe_3O_4–C60–WF microbubbles with different concentration on thrombosis are shown in Table 5. From Table 5, the wet weight and dry weight of thrombus decreased with the increase of microbubbles concentration. When the concentration of PLA–Tween composited Fe_3O_4–C60–WF microbubbles was 10 mg mL^{-1}, the wet and dry weight of thrombus were 236.91 ± 12.22 mg and 54.90 ± 9.54 mg, respectively, and there was no significant difference in comparison with that of 0 mg mL^{-1} ($P > 0.05$); when the concentration of composite microbubbles was 20 mg mL^{-1}, the thrombus wet weight was 210.20 ± 9.54 mg which was significantly different from that of 0 mg mL^{-1} ($P < 0.05$), the thrombus dry weight was 48.30 ± 2.29 mg, and there was no

Table 7 Influence of composite microbubbles with different concentrations on coagulation parameters

Concentration (mg mL^{-1})	PT	APTT	TT
0	9.1	30.5	11.5
10	10.1	31.5	12.4
20	10.2	32.6	12.9
40	10.4	34.3	13.0
60	11.0	34.7	13.1
80	13.2	35.9	14.6

significant difference in comparison with that of 0 mg mL^{-1} ($P > 0.05$); when the microbubbles concentration was 40 mg mL^{-1}, the wet weight and dry weight of thrombus were 207.53 ± 13.40 mg and 40.67 ± 6.67 mg, respectively, there were significantly difference in comparison with that of 0 mg mL^{-1} ($P < 0.05$); when the microbubbles concentration was 60 mg mL^{-1}, the thrombus wet weight was 196.47 ± 11.14 mg which was significantly different from that of 0 mg mL^{-1} ($P < 0.01$), the dry weight was 36.0 ± 4.85 mg while there was a significant difference ($P < 0.05$); when the microbubbles concentration was 80 mg mL^{-1}, wet weight and dry weight of thrombus were respectively 175.70 ± 9.88 mg and 32.73 ± 5.82 mg, which were significantly different from those of 0 mg mL^{-1} ($P < 0.01$). As a result, PLA–Tween composited Fe_3O_4–C60–WF microbubbles could effectively inhibit thrombosis *in vitro*.

PLA–Tween composited Fe_3O_4–C60–WF microbubbles with a concentration of 80 mg mL^{-1} were used for the subsequent studies. Inhibitory effects of different composite microbubbles on thrombus *in vitro* are shown in Table 6. From Table 6, the wet weight and dry weight of the thrombus for the normal saline control group were 241.13 ± 10.90 mg and 54.95 ± 5.04 mg, respectively. And the wet weight and dry weight of the thrombus for PLA–Tween microbubbles group were 237.30 ± 3.99 mg and 50.27 ± 1.33 mg, respectively, there was no statistical significance in comparison with the normal saline control group ($P > 0.05$), indicating that PLA–Tween microbubbles had no inhibitory effect on thrombosis *in vitro*. Wet weight and dry weight of thrombus for PLA–Tween composited C60–WF microbubble group were 187.43 ± 6.64 mg and 32.30 ± 5.31 mg, respectively, which were significantly different from that of the normal saline control group ($P < 0.01$); the thrombus wet weight for PLA–Tween composited C60–Fe_3O_4–WF microbubbles was 192.97 ± 8.97 mg, there was significantly difference in comparison with the normal saline control group ($P < 0.01$), and its thrombus dry weight was 36.00 ± 4.80 mg which was significantly different from that of normal saline control group ($P < 0.05$). It can be concluded that both PLA–Tween composited C60–WF microbubbles and PLA–Tween composited C60–Fe_3O_4–WF microbubbles had good inhibitory effects on thrombosis *in vitro*. There was no significant difference in the wet weight and dry weight of thrombus between PLA–Tween composited C60–WF microbubbles and PLA–Tween composited C60–Fe_3O_4–WF microbubbles group, indicating that Fe_3O_4 in PLA–Tween composited C60–Fe_3O_4–WF microbubbles had no significant effect on the antithrombotic performance of the composite microbubbles. The effects of composite microbubbles with different concentration on blood coagulation parameters are shown in Table 7. With the increase of the concentration of PLA–Tween composited C60–Fe_3O_4–WF microbubbles, the values of PT, TT and APTT of blood samples showed an increasing trend, which indicated that the inhibition effect of PLA–Tween composited C60–Fe_3O_4–WF microbubbles on thrombus was more obvious with the concentration increase.

Anticoagulation test results *in vitro* of different microbubbles were shown in Fig. 17. PLA–Tween microbubbles had no significant effect on APTT, TT and PT, indicating that it had no anticoagulant effect. Compared to the control group, the APTT, TT and PT values of PLA–Tween composited C60–WF microbubbles and PLA–Tween composited C60–Fe_3O_4–WF microbubbles were significantly increased, indicating that they could inhibit the formation of thrombus. There were no significant differences for APTT, TT and PT values between PLA–Tween composited C60–WF microbubbles and PLA–Tween composited C60–Fe_3O_4–WF microbubbles, indicating that Fe_3O_4 in PLA–Tween composited C60–Fe_3O_4–WF microbubbles had no significant effect on the anticoagulation effect of the composite microbubbles.

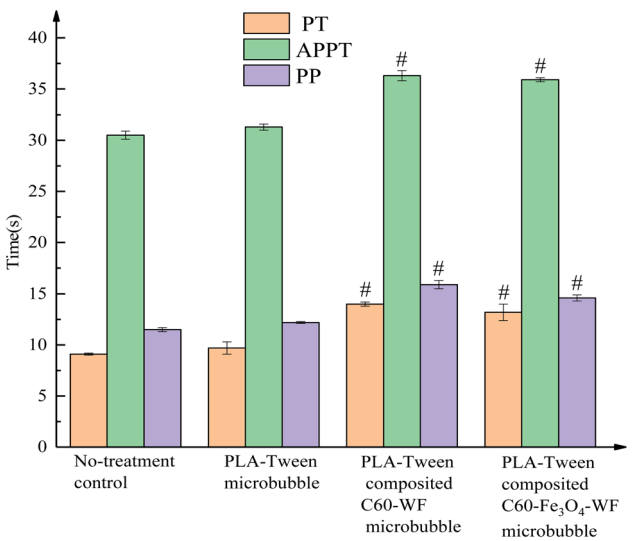

Fig. 17 Effects of different composite microbubbles on coagulation parameters. Note: compared to physiological saline group, "#" is $P < 0.01$.

3 Conclusions

The prepared PLA–Tween composited C60–Fe_3O_4 microbubbles had an average particle size of 446.4 nm and a Zeta potential of −40.5 mV. Its size was uniform and the stability was good, which could meet the needs of ultrasonic contrast agent. PLA–Tween composited C60–Fe_3O_4–DOX microbubbles could inhibit the growth of the breast cancer MDA-MB-231 cells and significantly reduced the toxicity of DOX alone on the normal cells. PLA–Tween composited C60–Fe_3O_4–NET microbubbles could inhibit the growth of *Staphylococcus aureus* and *Escherichia coli*, and the inhibitory effect on *Escherichia coli* was stronger than that on *Staphylococcus aureus*. PLA–Tween composited C60–Fe_3O_4–WF microbubbles could inhibit thrombosis, and significantly prolonged PT, TT and APTT. PLA–Tween composited C60–Fe_3O_4–DOX microbubbles on the rabbit kidney, PLA–Tween composited C60–Fe_3O_4–NET microbubbles on the rabbit bladder, PLA–Tween composited C60–Fe_3O_4–WF microbubbles on the rabbit abdominal aorta had good imaging performance. The effect of ultrasound imaging was enhanced under the magnetic field, and no adverse reactions occurred during the imaging process, which proved its good biological safety.

Conflicts of interest

There are no conflicts to declare.

Acknowledgements

This work was supported by National Natural Science Foundation of China (No. 81601616), science foundation of Heilongjiang province (No. LH2021H110), excellent innovation team based on the basic scientific research vocational cost for the provincial undergraduate universities in Heilongjiang (No. 2018-KYYWF-0914), scientific research initiation found of postdoctoral researchers settled down in Heilongjiang (No. 31303120), and innovation and entrepreneurship training program for college students in Heilongjiang province (No. 202010222053).

References

1 M. Shinichiro, T. Katsuro, O. Takahiro, *et al.*, In vitro transfer of antisense oligodeoxynucleotides into coronary endothelial cells by ultrasound, *Biochem. Biophys. Res. Commun.*, 2002, **298**, 587–590.

2 C. U. Evan, P. M. C. Thomas, H. S. Robert, *et al.*, In Vitro Studies of a New Thrombus-Specific Ultrasound Contrast Agent, *Am. J. Cardiol.*, 1998, **81**(12A), 58–61.

3 E. Jafarzadeh and A. N. Sinclair, Non-linear Wave Propagation and Safety Standards for Diagnostic Ultrasound Devices, *Ultrasound Med. Biol.*, 2019, **45**(1), 11–20.

4 Y. Fujita, T. O. Nakanishi, M. Sugitani, *et al.*, Placental Elasticity as a New Non-invasive Predictive Marker of Pre-eclampsia, *Ultrasound Med. Biol.*, 2019, **45**(1), 93–97.

5 S. Takiuchi, H. Rakugi, T. Masuyama, *et al.*, Clinical implications of ultrasonic tissue characterization for atherosclerotic carotid intima-media, *Nippon Ronen Igakkai Zasshi*, 2000, **37**(2), 137–142.

6 D. Pereira, C. Ferreira, R. Catarino, *et al.*, Hyperbaric oxygen for radiation-induced cystitis: a long-term follow-up, *Actas Urológicas Españolas*, 2020, **44**(8), 561–567.

7 X. Wang, H. Yin, L. Fan, *et al.*, Shionone alleviates NLRP3 inflammasome mediated pyroptosis in interstitial cystitis injury, *Int. Immunopharmacol.*, 2020, **90**, 427–436.

8 P. Loverlock, G. Haar, M. G. Ormerod, *et al.*, The effect of ultrasound on the cytotoxicity of adriamycin, *Br. J. Radiol.*, 1990, **63**(751), 542–546.

9 S. Umemura, K. Kawabata and K. Sasaki, In vitro and in vivo enhancement of sonodynamically active cavitation by second-harmonic superimposition, *J. Acoust. Soc. Am.*, 1997, **101**(1), 569–577.

10 G. Saba, D. R. Tatiana, C. João, *et al.*, Fullerene: biomedical engineers get to revisit an old friend, *Mater. Today*, 2017, **20**(8), 460–480.

11 W. A. James, D. Aleks, *et al.*, Photophysical properties of sixty atom carbon molecule (C60), *J. Phys.*, 1991, **95**(1), 11–12.